

Fluid inertia effects on the motion of small spherical bubbles or solid spheres in turbulent flows

Zhentong Zhang^{1,‡}, Dominique Legendre¹ and Rémi Zamansky^{1,†}

¹Institut de Mécanique des Fluides de Toulouse (IMFT), Université de Toulouse, CNRS, 31400 Toulouse, France

(Received 22 December 2020; revised 12 April 2021; accepted 10 May 2021)

In this paper we study finite particle Reynolds number effects up to $Re_p = 50$ on the dynamics of small spherical bubbles and solid particles in an isotropic turbulent flow. We consider direct numerical simulations of light pointwise particles with various expressions of the drag force to account for finite Re_p and the type of particle. Namely, we consider the Stokes drag law, the Schiller and Neumann relation and the Mei law. We show that an effective Stokes number, based on the mean value of the drag coefficient to account for the inertial effects involved in the drag law, gives a quasi-self-similar evolution of the variances of the bubble acceleration and of the forces exerted on the particle. This allows us to provide a satisfactory prediction of these quantities using Tchen's theory at finite particle Reynolds number. Based on these relations, we can specify the conditions under which the total inertial force (sum of the added mass and the Tchen contributions) is negligible compared with the drag force. Thus, for particles of very small dimensions, the fluid inertia force is negligible, provided the density ratio is of order 1 or larger. However, when the particle inertia becomes consequential, the threshold value of the density ratio increases significantly. Although this corresponds to the limit of the validity of the model, this draws attention to the fact that, for large Stokes numbers, the added mass and fluid inertia forces could play a more important role than is usually attributed to them.

Key words: bubble dynamics, particle/fluid flow, isotropic turbulence

1. Introduction

Predicting the dispersion of objects (particles, bubbles, droplets) in turbulent flows is very important in many circumstances both for engineering and natural applications. To achieve

† Email address for correspondence: remi.zamansky@imft.fr

‡ Present address: Laboratoire de Mathématiques Raphaël Salem, UFR des Sciences et Techniques, Université de Rouen Normandie, 76801 Saint-Étienne-du-Rouvray, France

this for small bodies, the pointwise particle approach (also called the Euler–Lagrange approach) is often considered. In this approach, the continuous fluid phase and the dispersed phase are computed separately and are coupled through momentum exchange. To close this momentum balance, one needs to provide an expression to calculate the hydrodynamic force acting on each dispersed object that both integrates the characteristics of the carrying flow and the response of the particle.

For the very specific situation of an isolated spherical particle, much smaller than the smallest spatial scale of the flow fluctuations, moving with a very small velocity relative to the carrier fluid such that its Reynolds number is vanishing, an exact formulation of the hydrodynamic force is known (Gatignol 1983; Maxey & Riley 1983). In the case of the finite Reynolds number, extension of unsteady dynamic forces on a spherical particle was proposed (Mei 1996; Magnaudet & Eames 2000). As in the creeping flow condition, the hydrodynamic force is decomposed into several terms including the stationary drag force, the history effects (or Basset–Boussinesq force), the lift force, the added mass effect and the inertia forces of the fluid (or Tchen force). The last two forces are due to the fluid inertia in non-stationary or non-uniform flow situations. Indeed, the added mass force results from the inertia of the volume of fluid that is accelerated by the displacement of the particle, while the Tchen force corresponds to the force that a volume of fluid would experience if it were in place of the particle and can be interpreted as a generalized buoyancy. Being purely inertial, these effects are independent of the particle Reynolds number (Rivero, Magnaudet & Fabre 1991) and involve the material derivative following a fluid element (Auton, Hunt & Prud’Homme 1988). The other hydrodynamic forces, namely the drag and the lift forces, while being essentially viscous effects in the limit of small particle Reynolds numbers, are nevertheless affected by the fluid inertia for intermediate Reynolds numbers, as evidenced by the explicit Reynolds number dependence of their expressions.

The relative importance of those forces in turbulent flows, as well as the effects of finite particle Reynolds number, remain mainly open questions. Usually one considers that, for spherical particles, the lift force can be neglected when the change in the ambient velocity field over the scale of the sphere is small compared with the velocity of the body relative to the flow (Calzavarini *et al.* 2008; Zhang 2019). The history force, or Basset force, which is expected to account for rapid transient effects in viscous flows, is shown to be negligible compared with the drag force (see for example Rivero *et al.* (1991) or Mei, Klausner & Lawrence (1994)) for clean bubbles and is usually neglected for solid particles with the argument that the kernel involved in the integral definition of this term quickly decays when the Reynolds number of the particle motion increases. The results of Calzavarini *et al.* (2012) indeed confirm the small effect of the history force on the dynamics of neutrally buoyant particles when using a short range kernel. Note, nevertheless, that Olivieri *et al.* (2014) report some effect of the history force on the heavy particles clustering in turbulent flow when using the slowly decaying kernel valid at zero Reynolds number. Finally let us mention that Volk *et al.* (2008) present a comparison between experiments and numerical simulations confirming that, considering the viscous drag, the added mass and Tchen forces enable us to obtain a good accuracy for the particle acceleration as long as the finite size can be ignored. Concerning the added mass and Tchen forces, their effects are usually considered as dominant for bubbles (Maxey, Chang & Wang 1994; Calzavarini *et al.* 2009; Prakash *et al.* 2012; Mathai *et al.* 2016; Zhang, Legendre & Zamansky 2019) and neutrally buoyant particles (Calzavarini *et al.* 2012) but it is generally supposed that, for heavy enough particles, they are negligible (Maxey & Corrsin 1986; Wang & Maxey 1993; Armenio & Fiorotto 2001; Bagchi & Balachandar 2003; Bec *et al.* 2006).

In this paper, we present direct numerical simulation (DNS) of light particles subject to added mass, Tchen and drag forces, transported by an isotropic and homogeneous turbulent flow. In order to analyse the effects of the fluid inertia on the particle dynamics for particle Reynolds numbers up to $O(100)$, we consider two finite particle Reynolds number corrections to the drag law relevant for solid particles and bubbles with diameter smaller than the dissipative length scale. We propose prediction for the particle Reynolds number, the drag force and for the fluid inertia forces (added mass effect and Tchen force) for the dispersion of small spherical particles in turbulent flows. Based on these relations, we clarify whether fluid inertia terms are negligible or not for a given density ratio and particle size.

In § 2, we discuss the modelling used for the particles and summarize the details of the numerical simulation. We present in § 3 our DNS results for various Stokes numbers and drag laws, and introduce an effective Stokes number that accounts for the finite Reynolds number effects on the particle response. In § 4 we recall the estimations for the variance of the acceleration and the particles forces presented in Zhang *et al.* (2019) and show that they can be combined with the effective Stokes number. In § 5 we discuss the importance of the fluid inertia forces with respect to the drag forces as the density ratio or the size of the particles is changed.

2. Modelling of particle dynamics

The objective is here to focus on finite Reynolds number effects on the small bubble or solid particle response in a turbulent flow. For that purpose, the viscous transient correction to the drag force and the lift force are neglected and the momentum balance equation for a small sphere with diameter d_p is then expressed as

$$m_p d_t \mathbf{u}_p = 2\pi\rho_f \nu d_p \phi(Re_p)(\mathbf{u}_f - \mathbf{u}_p) + m_f D_t \mathbf{u}_f + C_M m_f (D_t \mathbf{u}_f - d_t \mathbf{u}_p), \quad (2.1)$$

where $m_p = \pi\rho_p d_p^3/6$, $m_f = \pi\rho_f d_p^3/6$, ρ_p and ρ_f are the density of the particles and the fluid respectively, ν is kinematic viscosity and $C_M = 0.5$ is the added mass coefficient for a sphere; $d_t \mathbf{u}_p$ is the time derivative of the particle velocity and $D_t \mathbf{u}_f$ is the material derivative of the fluid velocity. Here, the fluid velocity and acceleration are evaluated at the particle position $\mathbf{u}_f = \mathbf{u}_f(\mathbf{x} = \mathbf{x}_p, t)$ and $D_t \mathbf{u}_f = D_t \mathbf{u}_f(\mathbf{x} = \mathbf{x}_p, t)$.

In (2.1), the first term on the right-hand side stands for the drag force \mathbf{f}_D that remains dominated by viscous effects up to $Re_p = O(100)$ where the particle Reynolds number $Re_p = |\mathbf{u}_f - \mathbf{u}_p|d_p/\nu$ is based on the slip velocity and the particle diameter. The correction $\phi(Re_p)$ accounts for finite Reynolds number effects but may also integrate other effects such as the interface mobility or contamination, the viscosity of a fluid particle as well as the particle shape. By definition, the case of a clean spherical bubble in the limit $Re_p \rightarrow 0$ (Hadamard 1911; Rybczynski 1911) will be in this paper the case of reference

$$\phi(Re_p) = 1. \quad (2.2)$$

Considering the drag coefficient defined as $\mathbf{f}_D = C_D \pi d_p^2 \rho_f |\mathbf{u}_f - \mathbf{u}_p| (\mathbf{u}_f - \mathbf{u}_p)/8$, any kind of particle can then be considered with $\phi(Re_p) = C_D/C_{D,0}$, where $C_{D,0} = 16/Re_p$ is the drag coefficient of a clean spherical bubble under the creeping flow condition (Hadamard 1911; Rybczynski 1911). Note also that, as a consequence of its definition, the Re_p -correction satisfies $\phi(Re_p) \geq 1$.

In this paper, two types of Re_p -corrections will be considered. The first one expresses the behaviour of clean spherical bubbles or spheres with a perfect slip condition (zero shear stress). For this type of particle, $\phi(Re_p)$ is obtained from the Mei *et al.* (1994) drag

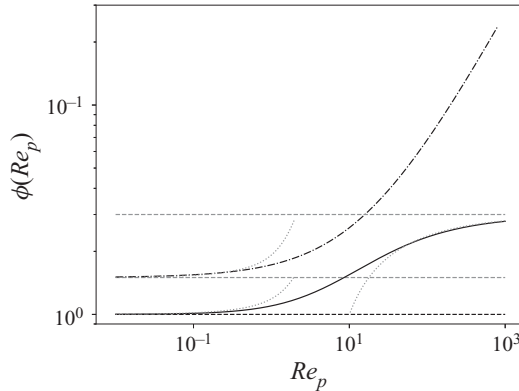


Figure 1. Some correction functions $\phi(Re_p)$ as a function of Re_p . For the spherical bubble case: relation (2.3) (continuous black line); the Stokes flow regime $\phi = 1$, defined in this paper as the case of reference (relation (2.2)) (black dashed line); the Taylor & Acrivos solution $\phi = 1 + Re_p/8$ (lower left dotted grey line); the Moore relation $\phi(Re_p) = 3[1 - 2.211Re_p^{-1/2}]$ (right dotted grey line); and the Levich relation $\phi(Re_p) = 3$ (upper grey dashed line). For the solid sphere case: the Stokes solution $\phi = 3/2$ (lower grey dashed line); the Oseen solution $\phi = 3/2(1 + 3Re_p/8)$ (upper left dotted grey line); and the Schiller and Naumann solution (2.4) (dash-dotted line).

force expression able to describe the drag force of a spherical bubble for any value of the Reynolds number

$$\phi(Re_p) = 1 + \left(\frac{8}{Re_p} + \frac{1}{2} \left(1 + \frac{3.315}{Re_p^{1/2}} \right) \right)^{-1}. \tag{2.3}$$

This relation is based on DNSs and has been built in order to recover in the limit $Re_p \rightarrow 0$ both $\phi(Re_p) = 1$ and $\phi(Re_p) = 1 + Re_p/8$ corresponding to the creeping flow solution (Hadamard 1911; Ryzczynski 1911) and the Oseen solution (Taylor & Acrivos 1964), respectively. In the limit of large Reynolds number, relation (2.3) recovers both $\phi(Re_p) = 3$ and $\phi(Re_p) = 3[1 - 2.211Re_p^{-1/2}]$ corresponding to the viscous potential solution of Levich (1962) and the boundary layer correction of Moore (1963), respectively. In the following, this type of Re_p -correction will be referred to as the spherical bubble case.

The second type of particle considered is a solid sphere with a no-slip surface or spherical bubble with a fully immobilized or contaminated interface. For this type of particle, the Re_p -correction is deduced from the drag coefficient of Schiller & Naumann (1933) valid for $Re_p < 800$

$$\phi(Re_p) = \frac{3}{2}(1 + 0.15Re_p^{0.687}). \tag{2.4}$$

This relation is based on an empirical fit of experimental data and tends to the Stokes solution for a solid sphere $\phi(Re_p) = 3/2$ in the limit $Re_p \rightarrow 0$ (Stokes 1851). In the following, this type of Re_p -correction will be referred to as the solid sphere case.

In figure 1, the above-listed functions $\phi(Re_p)$ are reported against the particle Reynolds number. As shown, the Re_p -correction increases faster for the solid sphere case (relation (2.4)) than for the spherical bubble case (relation (2.3)).

Rearranging (2.1), one obtains the momentum budget per unit of displaced/accelerated mass (i.e. accounting for the added mass effect) as

$$d_t \mathbf{u}_p = \frac{12\nu}{d_p^2(\rho_p/\rho_f + C_M)} \phi(Re)(\mathbf{u}_f - \mathbf{u}_p) + \beta D_t \mathbf{u}_f, \tag{2.5}$$

with $\beta = (1 + C_M)/(\rho_p/\rho_f + C_M)$ that compares the mass subject to the total fluid acceleration to the accelerated mass (Calzavarini *et al.* 2008; Toschi & Bodenschatz 2009; Mathai, Lohse & Sun 2020). In the following, the first and second terms on the left-hand side representing the drag and fluid inertia forces per unit of accelerated mass will be denoted by F_D ($F_D = \mathbf{f}_D/(m_p + C_M m_f)$) and F_I , respectively.

Based on (2.5), the characteristic particle relaxation time is defined as

$$\tau_p = \frac{1}{12} \left(\frac{\rho_p}{\rho_f} + C_M \right) \frac{d_p^2}{\nu}. \quad (2.6)$$

The Stokes number is then defined as the ratio between τ_p and the dissipative time scale of the flow τ_η

$$St = \frac{\tau_p}{\tau_\eta} = \frac{1}{12} \left(\frac{\rho_p}{\rho_f} + C_M \right) \left(\frac{d_p}{\eta} \right)^2, \quad (2.7)$$

with η the dissipative length scale of the turbulence. Note that the factor 1/12 in (2.6) and (2.7) is common for clean spherical bubbles in the limit $Re_p \rightarrow 0$, whereas, for solid particles, one usually has 1/18. Indeed, the change of stress condition at the interface is trivially accounted for by rescaling the Stokes number St as $St \rightarrow 2/3St$ when changing from a free-slip to a no-slip condition keeping the same flow conditions unchanged.

Accordingly, the non-dimensionalizing of the particle equation of motion by a reference velocity and the time scale τ_η reads

$$d_t \mathbf{u}_p = \phi(Re_p) \frac{\mathbf{u}_f - \mathbf{u}_p}{St} + \beta D_t \mathbf{u}_f. \quad (2.8)$$

As indicated by this equation, as $\phi(Re_p) \geq 1$, we expect to observe a faster response of the particles when considering finite Reynolds number effects.

In order for the above equation of motion to be valid, it is essential to consider that the flow around the particle is uniform at the particle scale. Therefore, in the context of homogeneous turbulence as considered in this study, we assume that the diameter of the particle remains sufficiently small compared with the scale of the smallest eddies. In practice, according to Calzavarini *et al.* (2009), it is sufficient to have $d_p/\eta < 10$.

The details of the numerical methods have been presented in Zhang *et al.* (2019). For the carrier phase, the homogeneous and isotropic turbulence is solved using a pseudo-spectral method with the large-scale forcing proposed by Kumar, Schumacher & Shaw (2014) given a Taylor scale Reynolds number of $Re_\lambda = 100$. A Lagrangian one-way coupling point-particle approach is considered for the particles with a Hermite interpolation scheme of the Eulerian field at the particle position. The flow conditions reported in table 1 are identical for the simulations of each type of particle considered. In the following, we analyse the effect of the finite Reynolds number for light spherical particles (bubble or solid particle) imposing $\rho_p/\rho_f = 0$ and $C_M = 0.5$, giving $\beta = 3$. For each set of simulations, we consider seven classes of particles with Stokes number ranging from 0.02 to 2, as listed in table 2.

In § 3, we investigate the finite Reynolds number effects on the dynamics of particles. For this, we consider for $\phi(Re_p)$ the expressions (2.2) (the case of reference with $\phi(Re_p) = 1$), (2.3) (the spherical bubble case) and (2.4) (the solid sphere case).

3. Finite Reynolds number effects and effective Stokes number

For the set of numerical simulations described in tables 1 and 2, we first report the statistics of the particle Reynolds number. Figure 2 shows the evolution of the mean

N	Re_H	Re_λ	T_L/τ_η	$\frac{\langle \varepsilon \rangle H}{\mathcal{K}^{3/2}}$	L/η	Re_0	η/Δ	$\Delta t/\tau_\eta$
512^3	2475	100	26	1.97	133	64	1.06	0.002

Table 1. The simulation parameters for the turbulent flow field. The number of grid points in each direction is N , $H = 2\pi$ the size of numerical domain, $T_L = (2/3\mathcal{K})/\varepsilon$ the eddy turnover time, $L = (2/3\mathcal{K})^{3/2}/\varepsilon$ the scale of the large eddies, \mathcal{K} the average turbulent kinetic energy and ε the average dissipation rate; $Re_H = H\sqrt{(2/3\mathcal{K})}/\nu$ is the Reynolds number based on the size of the computational domain, Re_λ is the Reynolds number based on the Taylor length scale, η and τ_η are the Kolmogorov length and time scales; $Re_0 = (\tau_L/\tau_\eta)^2$ is the square of the ratio of the Lagrangian integral time scale to the Kolmogorov time scale; Δ and Δt are the grid size and the time step of the simulation.

d_p/η	0.70	1.33	2.19	3.29	4.93	6.10	7.04
St	0.021	0.074	0.20	0.45	1.01	1.55	2.07

Table 2. The non-dimensional diameter of the particles d_p/η and their Stokes number St .

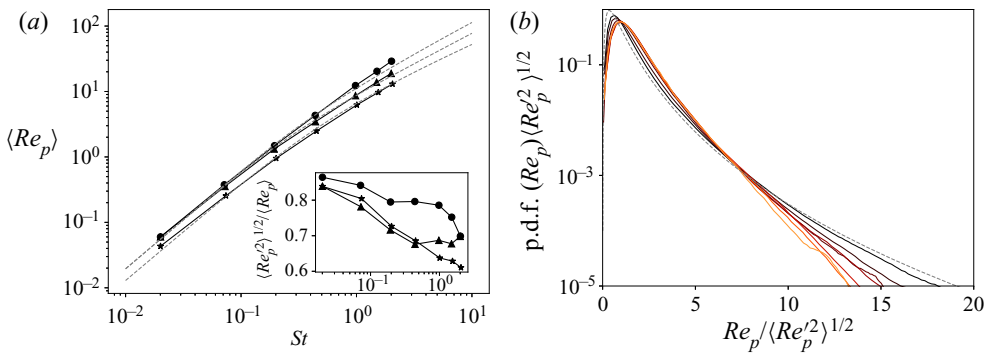


Figure 2. (a) Evolution of the mean particle Reynolds number with the Stokes number, for the three drag law considered here. Symbols represent the DNS, (o) the reference case $\phi(Re_p) = 1$, (Δ) spherical bubble case $\phi(Re_p)$ given by relation (2.3), (*) solid sphere case $\phi(Re_p)$ given by relation (2.4). The grey dashed line corresponds to the prediction of the Reynolds number proposed in (4.9). Inset: ratio of the standard deviation of the particle Reynolds number to its average. (b) The p.d.f. of Re_p for different St normalized by its standard deviation. For the case of the drag from Mei (2.3). Curves from black to orange correspond to an increase of the Stokes number. The dashed line is the log-normal distribution with parameters $\sigma^2 = \ln 2$, $\mu = -\sigma^2/2$, such that the mean and root-mean-square values are both unity.

and root-mean-square of the particle Reynolds number Re_p with St . As expected, for the three $\phi(Re_p)$ relations considered, the average value of the Reynolds number $\langle Re_p \rangle$ increases with the Stokes number. For $St > 1$, it appears that the average Reynolds number can be significantly larger than 1, which indicates that finite Reynolds number effects have a significant impact and should be accounted for. Indeed, we remark that the differences between the use of relation (2.2) or (2.3) are sizable at sufficiently large Stokes numbers, with a reduction of the relative velocity due to the Reynolds number effect. For the maximum Stokes number considered here, $\langle Re_p \rangle \approx 30$, when considering no Re_p -correction while $\langle Re_p \rangle \approx 20$ and $\langle Re_p \rangle \approx 10$ for spherical bubble (Re_p -correction

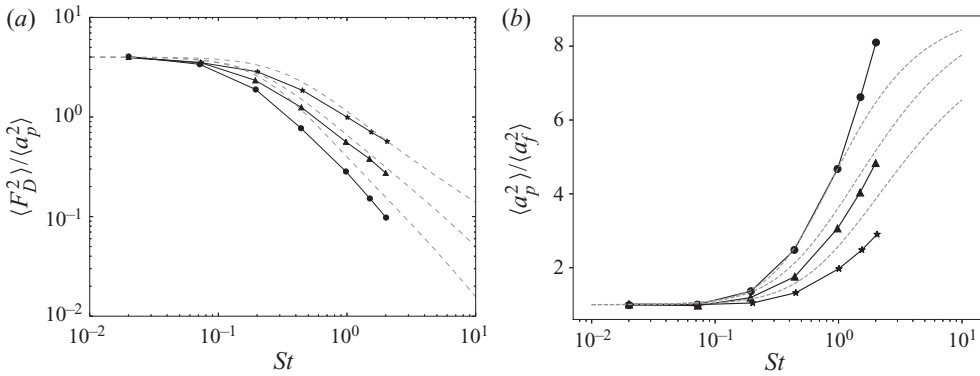


Figure 3. Variance of the drag force normalized by the variance of the particle acceleration (a) and variance of the acceleration normalized by the acceleration variance of fluid particles (b) as a function of the Stokes number St ; (○) obtained for a clean bubble in the Stokes flow regime (2.2), (△) for clean bubbles (2.3) and (*) for solid particles (2.4). The dashed lines correspond to expressions (4.5) and (4.7).

(2.3)) and solid sphere (Re_p -correction (2.4)) cases, respectively. As well, the relative velocity of a solid sphere is significantly reduced compared with a spherical bubble under the same flow conditions. We also remark in the inset of figure 2(a) that the standard deviation of the Reynolds number is of the order of its average value.

In figure 2(b), we report the probability distribution function (p.d.f.) of the Reynolds number when considering the Re_p -correction for the spherical bubble case (relation (2.3)). It is observed that the normalized p.d.f. is quite close to a log-normal distribution, and that the instantaneous Reynolds number can present deviations significantly larger than its root-mean-square. For $St \rightarrow 0$, the drag force and fluid inertia force are proportional (Zhang *et al.* 2019), leading the particle Reynolds number to be proportional to the norm of the fluid acceleration at the particle position: $Re_p = (d/\nu)\tau_p|1 - \beta||D_t \mathbf{u}_f|$. Therefore, the log-normal distribution of Re_p is expected since the fluid acceleration norm is well described by this distribution (Yeung *et al.* 2006; Toschi & Bodenschatz 2009). It is further observed that the normalized p.d.f. of Re_p depends slightly on the Stokes number, with a reduced probability of observing large Re_p fluctuations with increasing St . Note also that, for the two other considered cases, the behaviour (not presented in figure 2 for clarity) is very similar.

We present in figure 3 the variance of the drag forces per unit of accelerated mass F_D for the three different drag laws considered. Despite the increase of the relative velocity reported above, we observe that F_D is reduced when the Stokes number increases. We notice further that considering the Re_p -correction (2.3) gives a slower reduction compared with the case of reference $\phi(Re_p) = 1$. From the definition of the Reynolds number and of the Stokes number, F_D^2 normalized by the square of the Kolmogorov acceleration a_η^2 can be expressed as

$$\frac{F_D^2}{a_\eta^2} = \phi^2(Re_p) Re_p^2 \frac{\rho_p/\rho_f + C_M}{12} St^{-3}. \tag{3.1}$$

As indicated by this expression, if the quantity $\langle \phi^2(Re_p) Re_p^2 \rangle$ grows with St less rapidly than St^3 , then the variance of F_D^2/a_η^2 decreases as the Stokes number increases, as observed in figure 3. When considering the solid sphere case, which presents the strongest increase

of the correction function ϕ with Re_p , this imposes that $\langle Re_p \rangle$ grows approximately slower than linearly, as already observed in [figure 2](#).

In [figure 3](#) we also report the particle acceleration variance $\langle a_p^2 \rangle$. It is observed that, for the three drag laws considered, the acceleration variance normalized by the fluid acceleration variance $\langle a_f^2 \rangle$ increases with the Stokes number, essentially due to the progressive fading of the drag force as well as its decorrelation with the fluid inertia force, as explained by Zhang *et al.* (2019). Note that further increase of the Stokes number would lead to a saturation of the normalized acceleration variance to β^2 , as shown by Calzavarini *et al.* (2009) and Zhang *et al.* (2019), but in this case the particle diameter would be too large for the pointwise particle approach to remain valid. The case of reference $\phi(Re_p) = 1$ gives to a faster increase of the acceleration variance and for the case of spherical bubbles it increases faster than for the solid sphere case.

To characterize the inertia effects on the particle response time through the drag force correction $\phi(Re_p)$, we decompose the particle Reynolds number into its mean and fluctuating parts, $Re_p = \langle Re_p \rangle + Re'_p$ and approximate the drag force per unit of accelerated mass using a Taylor expansion of the function ϕ around $\phi(\langle Re_p \rangle)$

$$F_D = \phi(\langle Re_p \rangle) \frac{\mathbf{u}_f - \mathbf{u}_p}{\tau_p} + Re'_p \phi'(\langle Re_p \rangle) \frac{\mathbf{u}_f - \mathbf{u}_p}{\tau_p} + \dots, \quad (3.2)$$

with ϕ' the derivative of ϕ with respect to Re_p . This relation leads to the introduction of an effective relaxation time τ_p^* , as already proposed by Février, Simonin & Squires (2005) and Bergougnoux, Bouchet & Lopez (2014), that accounts for the Reynolds number effects

$$\tau_p^* = \tau_p / \phi(\langle Re_p \rangle). \quad (3.3)$$

We further introduce the effective Stokes number as

$$St_* = St / \phi(\langle Re_p \rangle). \quad (3.4)$$

Despite the particle Reynolds number presenting large fluctuations, the Taylor expansion can be truncated at first order as far as one is concerned with low-order statistics. To justify this assertion, we compare the magnitude of the second-order and the first-order terms in (3.2). We plot in [figure 4](#) the ratio $\langle Re_p \rangle \phi'(\langle Re_p \rangle) / \phi(\langle Re_p \rangle)$ against $\langle Re_p \rangle$ for the two Re_p -corrections considered here (2.3)–(2.4). Note that this amounts to considering that the order of magnitude of the fluctuations of Re_p as $O(Re'_p) = \langle Re_p \rangle$, consistently with the observation of [figure 2](#). We remark that for the case of reference $\phi'(\langle Re_p \rangle) = 0$. We found that, in the simulation for spherical bubbles, the largest value of this ratio is approximately 0.2 for $St \approx 1.55$ and in the simulation for a solid sphere, the ratio increases monotonically up to its asymptotic value of 0.687 at large St . For moderate values of Reynolds number, the second term on the right-hand side of (3.2) remains smaller than the first term.

In order to discuss the relevance of St_* , we show in [figure 5](#) the evolution of the variance of the drag force and of the particle acceleration for the various simulations as a function of St_* . When plotted against St_* , these quantities now collapse onto a single curve, compared with what is reported in [figure 3](#) where the evolution is reported against St . We recover here the expected effect of the Re_p -correction on the drag force: the particle response time to the flow is decreased, thus decreasing the effective Stokes number. We show that the effective Stokes number given by (3.4) is the relevant parameter to describe the inertial flow effect on the particle response to the turbulent flow.

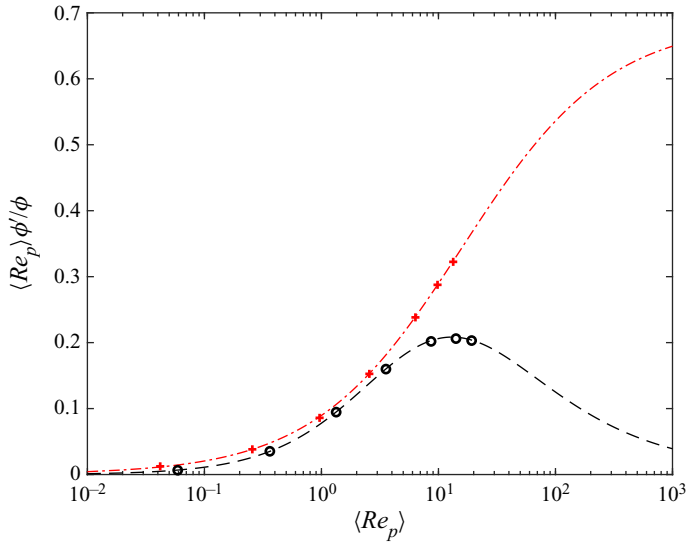


Figure 4. Evolution of $(\langle Re_p \rangle / \phi(\langle Re_p \rangle)) \phi'(\langle Re_p \rangle)$ as a function of $\langle Re_p \rangle$. Symbols correspond to the results of the DNS: (o) for the bubble case with the Mei *et al.* (1994) correction (2.3); (x) for the solid sphere case with the Schiller & Naumann (1933) correction (2.4). The lines are the analytical results corresponding to (2.3) (in red) and (2.4) (in black).

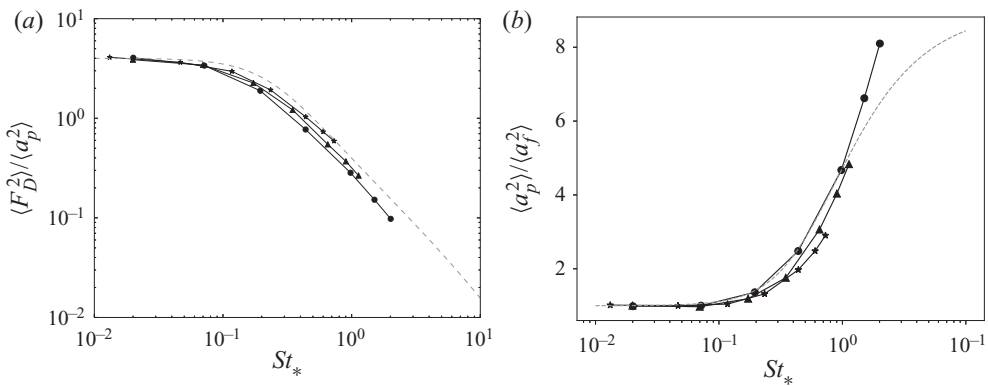


Figure 5. Variance of the drag force normalized by the variance of the particle acceleration (a) and variance of the acceleration normalized by the acceleration variance of fluid particles (b) as a function of the modified Stokes number St_* : (o) obtained with no Re_p -corrections, (Δ) for clean bubbles (2.3) and ($*$) for solid particles (2.4). The dashed lines correspond to the estimation from (4.5) and (4.7).

4. Prediction for the forces applied to the particle and the Reynolds number

Following the approach of Tchen (1947) (see also Hinze 1975; Mei 1996; Alipchenkov & Zaichik 2010), Zhang *et al.* (2019) estimate the variance of the drag forces, the fluid inertia force and the particle acceleration variance as functions of St , β and a Reynolds number $Re_0 = (\tau_L / \tau_\eta)^2$ defined as the square of the ratio of the Lagrangian integral time scale τ_L

to the Kolmogorov time scale, as

$$\frac{\langle F_D^2 \rangle}{a_\eta^2} \approx c_0 \frac{(1 - \beta)^2}{1 - St^2/Re_0} \left[\frac{\tan^{-1}(c_1 St)}{c_1 St} - \frac{\tan^{-1}(c_1 Re_0^{1/2})}{c_1 Re_0^{1/2}} \right] = \Gamma_D(St, \beta, Re_0), \quad (4.1)$$

$$\frac{\langle F_I^2 \rangle}{a_\eta^2} \approx c_0 \beta^2 \left[1 - \frac{\tan^{-1}(c_1 Re_0^{1/2})}{c_1 Re_0^{1/2}} \right] = \Gamma_I(St, \beta, Re_0), \quad (4.2)$$

$$\begin{aligned} \frac{\langle a_p^2 \rangle}{a_\eta^2} &\approx c_0 \left[\beta^2 + \frac{1 - \beta^2}{1 - St^2/Re_0} \frac{\tan^{-1}(c_1 St)}{c_1 St} - \frac{1 - \beta^2 St^2/Re_0}{1 - St^2/Re_0} \frac{\tan^{-1}(c_1 Re_0^{1/2})}{c_1 Re_0^{1/2}} \right] \\ &= \Gamma_a(St, \beta, Re_0), \end{aligned} \quad (4.3)$$

with the parameter c_1 found to be $c_1 = 2.1$; c_0 can be interpreted as the ratio of the fluid particle acceleration variance to the square of the Kolmogorov acceleration, and is therefore dependent on the flow Reynolds number, as reported for example by La Porta *et al.* (2001) and Sawford *et al.* (2003). Note that Re_0 can be approximated as $Re_0 \approx (0.08 Re_\lambda)^2$ (Sawford & Yeung 2011; Zhang *et al.* 2019). In (4.1), (4.2) and (4.3) we introduce Γ_D , Γ_I and Γ_a as the estimations for $\langle F_D^2 \rangle/a_\eta^2$, $\langle F_I^2 \rangle/a_\eta^2$ and $\langle a_p^2 \rangle/a_\eta^2$, respectively. These expressions are valid for $Re_p \ll 1$ as they are based on a linear response of the particle velocity to the fluid velocity. Further, in the derivation of these expressions, two main assumptions are considered. Firstly, we assume that the Lagrangian fluid velocity spectra along the trajectory can be modelled as (Hinze 1975; Mordant, Metz & Michel 2001)

$$E_f(\omega) = \begin{cases} \frac{k_0 \tau_L^2 \langle \varepsilon \rangle}{(\tau_L \omega)^2 + 1} & \text{for } \omega < k_1 \frac{2\pi}{\tau_\eta}, \\ 0 & \text{for } \omega \geq k_1 \frac{2\pi}{\tau_\eta}, \end{cases} \quad (4.4)$$

which presents saturation for $\omega \ll \tau_L^{-1}$. The coefficients k_1 and k_0 are such that $c_0 = 2\pi k_1 k_0$ and $c_1 = 2\pi k_1$. The second assumption amounts to substituting the material derivative of the fluid velocity at the particle position by the Lagrangian time derivative along the particle trajectory, in order to obtain a close expression depending only on the value of the fluid velocity at the particle position. Zhang *et al.* (2019) checked that these assumptions are valid in the case of bubbles with a sufficiently small Reynolds number. In particular, it was shown that the first assumption gives a quite accurate acceleration variance although it misses any effect of preferential concentration while the second one requires the Stokes number to be sufficiently small to be valid.

We propose to generalize the relations (4.1)–(4.3) to the cases of particles with a finite Reynolds number. For this, we take into account their nonlinear drag law (Re_p -correction) by relying on the effective particle response time introduced in the previous section. Indeed, in view of the similarity of the evolution of the variance of the force and the acceleration as a function of St_* , presented in figure 5, we simply propose to replace St by

$St_* = St/\phi(\langle Re \rangle)$ in (4.1)–(4.3)

$$\frac{\langle F_D^2 \rangle}{a_\eta^2} \approx \Gamma_D(St_*, \beta, Re_0), \quad (4.5)$$

$$\frac{\langle F_I^2 \rangle}{a_\eta^2} \approx \Gamma_I(St_*, \beta, Re_0), \quad (4.6)$$

$$\frac{\langle a_p^2 \rangle}{a_\eta^2} \approx \Gamma_a(St_*, \beta, Re_0). \quad (4.7)$$

Note that (4.6) is left unchanged, since in our basic approximation the fluid particle acceleration at the particle position does not depend on the Stokes number as preferential concentration effects are discarded, $\Gamma_I(St_*, \beta, Re_0) = \Gamma_I(\beta, Re_0)$.

The issue, for the use of these relations, is now to have a prediction for St_* , as it requires us to know the average particle Reynolds number $\langle Re_p \rangle$. First of all, we observe in figure 2 that the standard deviation of the Reynolds number is nearly equal to its average, and as a consequence one can write $\langle Re_p \rangle \approx \sqrt{\langle Re_p^2 \rangle}/2$. On the other hand, it follows from the previous section that the variance of the drag force can be estimated, at first order, as $\langle F_D^2 \rangle \approx \langle (\mathbf{u}_p - \mathbf{u}_f)^2 \rangle / \tau_p^{*2}$. Substituting in the estimation of the average Reynolds number, we obtain

$$\langle Re_p \rangle \approx St_* \frac{d_p}{\eta} \sqrt{\frac{1}{2} \frac{\langle F_D^2 \rangle}{a_\eta^2}}. \quad (4.8)$$

Further, using the estimate of the drag force variance (4.5) and substituting with the definition of St_* from relation (3.4), we obtain an implicit relation that makes possible the calculation of $\langle Re_p \rangle$

$$\langle Re_p \rangle \approx \frac{St}{\phi(\langle Re_p \rangle)} \frac{d_p}{\eta} \left[\frac{1}{2} \Gamma_D(St/\phi(\langle Re_p \rangle), \beta, Re_0) \right]^{1/2}. \quad (4.9)$$

This expression can easily be solved iteratively by taking for example as initial guess $\langle Re_p \rangle = 0$. We present in figure 2 the comparison between the calculation of $\langle Re_p \rangle$ from (4.9) and the values obtained by DNS. It is observed that, for the three drag laws considered here, the estimation of the average particle Reynolds number is close to the DNS value. We also show in figures 3 and 5 the comparison to the DNS for the variances of the drag force and of the particle acceleration for the three drag laws. We can conclude that the relations (4.5)–(4.9) provide overall a good prediction of the variance of the considered quantities. Note that, for $St_* \approx 1$, (4.7) underestimates the acceleration variance but if St_* is further increased we find the saturation of the acceleration variance as presented in Zhang *et al.* (2019) and Calzavarini *et al.* (2009).

5. Relevance of fluid inertia force for small particles in turbulent flows

The fluid inertia force is dominant in the dynamics of light particles ($\rho_p/\rho_f \ll 1$). On the other hand, it is usually accepted that, for very dense particles ($\rho_p/\rho_f \gg 1$), the fluid inertia force is unimportant. This suggests that only the density ratio matters to justify neglecting the role of the inertia force in the momentum balance of a particle.

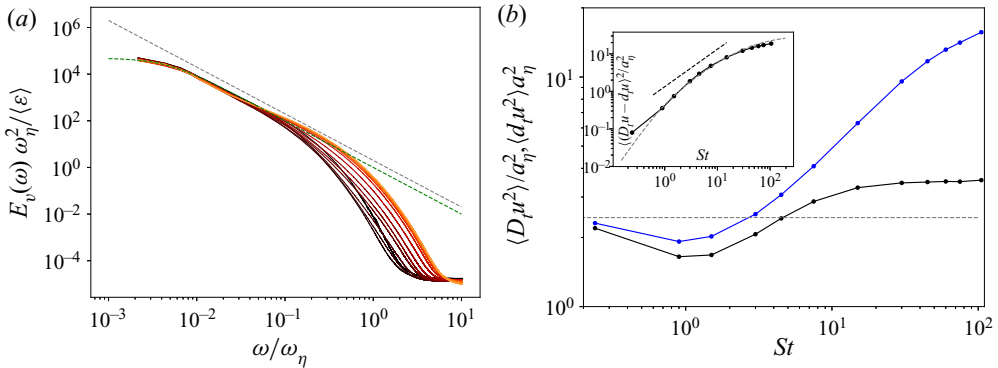


Figure 6. (a) Temporal spectra of the fluid velocity along the particle trajectory, for heavy particles only subject to the drag forces with the Stokes drag (i.e. $\phi(Re_p) = 3/2$), for $Re_\lambda = 400$ and $St = 0.24, 0.9, 1.5, 3., 4.5, 7.5, 15, 30, 45, 60, 75, 105$, from black to orange respectively from the DNS dataset of Bec *et al.* (2010) and Lanotte *et al.* (2011) in comparison with the power law ω^{-2} in grey dashed line and with the model spectra (4.4) in green dashed line. (b) Evolution with St of the variance of the material derivative of the fluid velocity at the particle position $D_t \mathbf{u}_f$ (in black) compared to the Lagrangian derivative of the fluid along the particle trajectory $d_t \mathbf{u}_f$ (in blue) for heavy particles (same dataset as a). Comparison with the prediction of (4.6) for $\beta^2 = 1$ in grey dashed line. Inset: variance of $D_t \mathbf{u}_f - d_t \mathbf{u}_f$ and comparison to $St_*^2 \langle F_D^2 \rangle$ computed from relation (4.5).

Using estimates (4.5) and (4.6) for the drag force and the inertia force, we show in the following that this condition could be more subtle and also depends on the particle size.

Before using these relations, we first verify that the underlying assumptions, recalled previously and validated for $\rho_p/\rho_f \rightarrow 0$ by Zhang *et al.* (2019), remain relevant for large density ratios. For this, we show in figure 6 the temporal spectrum of the fluid velocity along the trajectories of solid particles with a high density ratio. To plot this figure we have used data from the DNS of homogeneous isotropic turbulence of Bec *et al.* (2010) and Lanotte *et al.* (2011) obtained for twelve Stokes numbers between $St = 0.24$ and 105 (with St defined as (2.7)) for a homogeneous and isotropic turbulent flow at $Re_\lambda = 400$. For these simulations the solid particles are only subjected to the Stokes drag force (i.e. $\phi(Re_p) = 3/2$). We see in this figure that, even for the largest Stokes numbers, the velocity spectrum is well described by relation (4.4). The effect of the Stokes number is only visible at high frequencies.

The second assumption made to derive equations (4.5) and (4.6) neglects the term $(\mathbf{u}_p - \mathbf{u}_f) \cdot \nabla \mathbf{u}_f$, in order to identify the material derivative of the fluid velocity $D_t \mathbf{u}_f$ with its derivative along particle trajectories $d_t \mathbf{u}_f$, $D_t \mathbf{u}_f = d_t \mathbf{u}_f - (\mathbf{u}_p - \mathbf{u}_f) \cdot \nabla \mathbf{u}_f$. We show in figure 6 that this assumption becomes more and more inaccurate as the Stokes number increases since the particles trajectory diverges from the trajectory of a fluid particle. The difference between $D_t \mathbf{u}_f$ and $d_t \mathbf{u}_f$ can be estimated by assuming that $(\mathbf{u}_p - \mathbf{u}_f)$ and $\nabla \mathbf{u}_f$ are independent, the first being estimated using relations (3.2) and (4.5) and the second being of the order of $1/\tau_\eta$, which gives $\langle (D_t \mathbf{u}_f - d_t \mathbf{u}_f)^2 \rangle \approx St_*^2 \langle F_D^2 \rangle$. In the inset of figure 6 we see that this estimate is relatively accurate, except for the smallest Stokes numbers for which $(\mathbf{u}_p - \mathbf{u}_f)$ and $\nabla \mathbf{u}_f$ are not independent. From this estimate, we conclude that the difference between $D_t \mathbf{u}_f$ and $d_t \mathbf{u}_f$ remains bounded even for very large Stokes numbers, since $\langle F_D^2 \rangle$ decreases as St_*^{-2} for $St_* \gg Re_0^{1/2}$. Moreover, it worth remarking that the variance of the material derivative of the fluid velocity at the particle position remains roughly constant when St varies (its variations remain in a $\pm 30\%$ range). Therefore relation (4.6), which predicts F_I as independent of St , appears to be in agreement

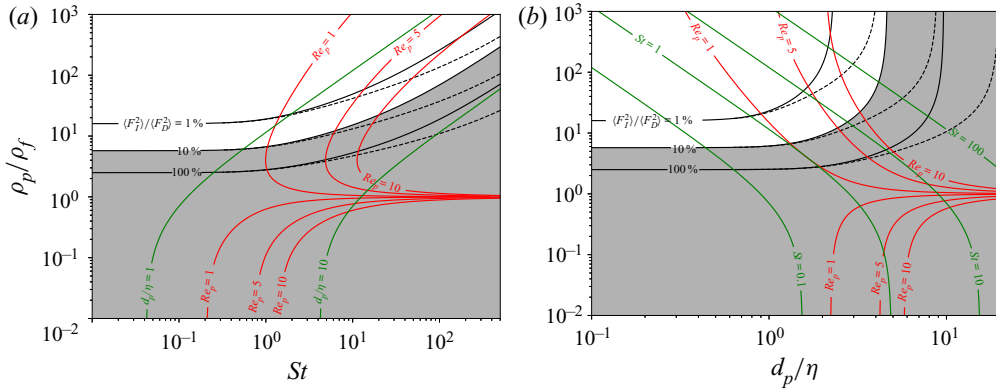


Figure 7. Diagram reporting the evolution of $\langle F_I^2 \rangle / \langle F_D^2 \rangle$. Iso-values 0.01, 0.1 and 1, of the ratio estimated by (4.5) and (4.6) for $Re_\lambda = 100$ (continuous black lines) and $Re_\lambda = 400$ (dashed lines) as a function of ρ_p / ρ_f and St (a) and as a function of ρ_p / ρ_f and d_p / η (b). The red lines indicate iso-values of the particles Reynolds number from (4.9) for $Re_\lambda = 100$. Green lines give iso-values of d_p / η (a) and of St (b). The region of the map where $\langle F_I^2 \rangle / \langle F_D^2 \rangle > 0.1$ is shaded.

with the DNS. This indicates that the two approximations discussed previously tend to compensate each other. Finally, let us mention that in Zhang *et al.* (2019) it can be checked that relation (4.5) makes a good estimate of the variance of the drag forces for heavy particles.

In figure 7, the ratio of $\langle F_I^2 \rangle / \langle F_D^2 \rangle$ estimated from (4.5) and (4.6) is plotted for a range of density ratios and particle sizes. For this figure we have selected the Re_p -correction (2.4) corresponding to the drag force of a solid sphere given by the relation of Schiller and Neuman. We plot 3 levels of the force ratio $\langle F_I^2 \rangle / \langle F_D^2 \rangle = 1\%$, 10% and 100% vs ρ_p / ρ_f and St in figure 7(a). In this plot, the region of the parameter map for which it is important to account for the fluid inertia forces is shaded in grey. This region is arbitrarily delimited by the curve corresponding to $\langle F_I^2 \rangle / \langle F_D^2 \rangle = 10\%$. It should be noted that the intermittency is not taken into account, and since the fluid acceleration fluctuations can be much greater than its standard deviation, it tends to further strengthen the effect of the fluid inertia force. Additionally, we plot some levels of the particle Reynolds number as calculated using relation (4.9). As expected, it is observed that, for light particles ($\rho_p / \rho_f < 1$), the fluid inertia force is dominant, whereas, for heavy particles, $\rho_p / \rho_f > 1$, we observe that the fluid inertia force can be neglected for $\rho_p / \rho_f > 10$ and small enough particle diameter, typically $St < 1$. However, when the particle Stokes number is increased, the density ratio also needs to be increased in order to neglect the effect of the fluid inertia force. Typically, one needs $\rho_p / \rho_f > 100$ for $St = 100$. The non-vanishing effect of the fluid inertia force for very heavy but large particles can be simply explained by the observation that, at first order, the fluid inertia force (per unit of displaced mass) is independent of the particles size, as long as the finite size effects can be ignored, while the magnitude of the drag force (per unit of displaced mass) decreases with the particle size, as shown in figure 3.

Furthermore, considering the plot against ρ_p / ρ_f and d_p / η given in figure 7(b), we can remark that, at $Re_\lambda = 100$ for particles of size $d_p / \eta \approx 3$, the inertia force remains important even for very large density ratios. This observation depends on the Reynolds number of the flow. Indeed, for $Re_\lambda = 400$, the fluid inertia force should not be neglected for a particle larger than $d_p / \eta \approx 7$. Since it was proposed by Calzavarini *et al.* (2009) that

the finite size effect can be disregarded for particles smaller than $d_p/\eta \approx 10$, the results presented in this section points out that the added mass force can turn out to be of the order of magnitude of the drag force, when the particle inertia becomes important, even for high density ratios. It is interesting to note that the occurrence of this range of size for which the fluid inertia force might be important is also the limit of the validity of the pointwise particle approach. Indeed, for larger particles ($d_p/\eta > 10$) one should account for the finite size effect, probably by considering the filtering at the scale of the particles of the fluid inertia force as proposed by Calzavarini *et al.* (2009), as well as the additional agitation caused by the turbulent structure of the flow around the particles by introducing a random drag coefficient (Gorokhovski & Zamansky 2018), which leads both variances of the drag force and of the inertia force to scale as $a_\eta^2(d/\eta)^{-2/3}$ (without accounting for the intermittency correction) as shown from the experimental results presented by Voth *et al.* (2002), Qureshi *et al.* (2008) and Volk *et al.* (2011).

6. Conclusion

We have analysed by DNS with the Euler–Lagrange framework, the effect of finite Reynolds number on the motion of small particles in a homogeneous and isotropic turbulent flow by considering two types of particles (spherical bubble and solid sphere), characterized by different Re_p -corrections in the drag force. We observe that the finite Reynolds number effects can be accounted for at first order by introducing an effective Stokes number based on the average particle Reynolds number. This rescaling of the particles time scale gives a quasi-self-similar evolution of the variances of the particle acceleration and of the forces exerted on it which can be satisfactorily estimated using Tchen’s theory. On the basis of these new expressions of the forces and acceleration of the particles, we confirm that the fluid inertia force is negligible compared with the drag force for particles of very small dimensions when the density ratio is of order 1 or larger. However, we show that, for significant particle inertia, the fluid inertia force is important unless the density ratio is increased significantly. Although this corresponds to the limit of the validity of the pointwise approach, this points out that, for large particles, the added mass and fluid inertia forces can be relevant.


It should also be noted that, as the particle size increases, forces other than the fluid inertia forces can also become important. In particular, gravity must often be considered for particles with large inertia. Indeed Mathai *et al.* (2016) have shown that for $St/Fr > 1$, with $Fr = a_\eta/g$ the Froude number, gravity g influences the trajectory of the particles. In this case, the particle Reynolds number can become significantly larger than 1, because of the large relative velocity experienced by the particles. The finite Reynolds number effect of the drag force is expected to reduce the average rising velocity by increasing the mean drag force. Finally, we can use the effective relaxation time introduced in this paper to take into account finite Reynolds number effects in estimating the terminal velocity of particles.

Acknowledgements. We thank A. Lanotte, E. Calzavarini, F. Toschi, J. Bec, L. Biferale and M. Cencini for making the DNS dataset ‘Heavy particles in turbulent flows’ (2011) publicly available from the International CFD Database (Lanotte *et al.* 2011).

Funding. Our DNS simulations were performed using high-performance computing resources from GENCI-CINES and GENCI-IDRIS (grant A0092B07400) and the CALMIP Centre of the University of Toulouse (grant P0910).

Declaration of interests. The authors report no conflict of interest.

Author ORCIDs.

-  Zhentong Zhang <https://orcid.org/0000-0002-0070-4580>;
 Dominique Legendre <https://orcid.org/0000-0002-6021-7119>;
 Rémi Zamansky <https://orcid.org/0000-0001-6704-5316>.

REFERENCES

- ALIPCHENKOV, V.M. & ZAICHIK, L.I. 2010 Modeling of the motion of light-weight particles and bubbles in turbulent flows. *Fluid Dyn.* **45** (4), 574–590.
- ARMENIO, V. & FIOROTTO, V. 2001 The importance of the forces acting on particles in turbulent flows. *Phys. Fluids* **13** (8), 2437–2440.
- AUTON, T.R., HUNT, J.C.R. & PRUD'HOMME, M. 1988 The force exerted on a body in inviscid unsteady non-uniform rotational flow. *J. Fluid Mech.* **197**, 241–257.
- BAGCHI, P. & BALACHANDAR, S. 2003 Effect of turbulence on the drag and lift of a particle. *Phys. Fluids* **15** (11), 3496–3513.
- BEC, J., BIFERALE, L., BOFFETTA, G., CELANI, A., CENCINI, M., LANOTTE, A., MUSACCHIO, S. & TOSCHI, F. 2006 Acceleration statistics of heavy particles in turbulence. *J. Fluid Mech.* **550**, 349–358.
- BEC, J., BIFERALE, L., CENCINI, M., LANOTTE, A. & TOSCHI, F. 2010 Intermittency in the velocity distribution of heavy particles in turbulence. *J. Fluid Mech.* **646**, 527–536.
- BERGOUGNOUX, L., BOUCHET, G., LOPEZ, D. & GUAZZELLI, É. 2014 The motion of solid spherical particles falling in a cellular flow field at low Stokes number. *Phys. Fluids* **26** (9), 093302.
- CALZAVARINI, E., KERSCHER, M., LOHSE, D. & TOSCHI, F. 2008 Dimensionality and morphology of particle and bubble clusters in turbulent flow. *J. Fluid Mech.* **607**, 13–24.
- CALZAVARINI, E., VOLK, R., BOURGOIN, M., LÉVÊQUE, E., PINTON, J.-F. & TOSCHI, F. 2009 Acceleration statistics of finite-sized particles in turbulent flow: the role of Faxén forces. *J. Fluid Mech.* **630** (-1), 179–189.
- CALZAVARINI, E., VOLK, R., LÉVÊQUE, E., PINTON, J.-F. & TOSCHI, F. 2012 Impact of trailing wake drag on the statistical properties and dynamics of finite-sized particle in turbulence. *Physica D* **241** (3), 237–244.
- FÉVRIER, P., SIMONIN, O. & SQUIRES, K.D. 2005 Partitioning of particle velocities in gas–solid turbulent flows into a continuous field and a spatially uncorrelated random distribution: theoretical formalism and numerical study. *J. Fluid Mech.* **533**, 1–46.
- GATIGNOL, R. 1983 The Faxén formulae for a rigid particle in an unsteady non-uniform Stokes flow. *J. Méc.* **1**, 143–160.
- GOROKHOVSKI, M. & ZAMANSKY, R. 2018 Modeling the effects of small turbulent scales on the drag force for particles below and above the Kolmogorov scale. *Phys. Rev. Fluids* **3** (3), 1–23.
- HADAMARD, J.S. 1911 Mouvement permanent lent d'une sphere liquide et visqueuse dans un liquide visqueux. *C. R. Acad. Sci. Paris* **152**, 1735.
- HINZE, J.O. 1975 *Turbulence*, 2nd edn. McGraw-Hill.
- KUMAR, B., SCHUMACHER, J. & SHAW, R.A. 2014 Lagrangian mixing dynamics at the cloudy–clear air interface. *J. Atmos. Sci.* **71** (7), 2564–2580.
- LA PORTA, A., VOTH, G.A., CRAWFORD, A.M., ALEXANDER, J. & BODENSCHATZ, E. 2001 Fluid particle accelerations in fully developed turbulence. *Nature* **409**, 1017–1019.
- LANOTTE, A., CALZAVARINI, E., FEDERICO, T., JEREMIE, B., LUCA, B. & MASSIMO, C. 2011 Heavy particles in turbulent flows. Dataset, International CFD Database.
- LEVICH, V.G. 1962 *Physicochemical Hydrodynamics*. Prentice-Hall.
- MAGNAUDET, J. & EAMES, I. 2000 The motion of high-Reynolds-number bubbles in inhomogeneous flows. *Annu. Rev. Fluid Mech.* **32**, 659–708.
- MATHAI, V., CALZAVARINI, E., BRONS, J., SUN, C. & LOHSE, D. 2016 Microbubbles and microparticles are not faithful tracers of turbulent acceleration. *Phys. Rev. Lett.* **117**, 024501.
- MATHAI, V., LOHSE, D. & SUN, C. 2020 Bubble and buoyant particle laden turbulent flows. *Annu. Rev. Condens. Matter Phys.* **11**, 1–38.
- MAXEY, M.R., CHANG, E.J. & WANG, L.-P. 1994 Simulation of interactions between microbubbles and turbulent flows. *Appl. Mech. Rev.* **47** (6S), S70–S74.
- MAXEY, M.R. & CORRSIN, S. 1986 Gravitational settling of aerosol particles in randomly oriented cellular flow fields. *J. Atmos. Sci.* **43** (11), 1112–1134.
- MAXEY, M.R. & RILEY, J.J. 1983 Equation of motion for a small rigid sphere in a nonuniform flow. *Phys. Fluids* **26** (4), 883–889.

- MEI, R. 1996 Velocity fidelity of flow tracer particles. *Exp. Fluids* **22** (1), 1–13.
- MEI, R., KLAUSNER, J.F. & LAWRENCE, C.J. 1994 A note on the history force on a spherical bubble at finite Reynolds number. *Phys. Fluids* **6**, 418.
- MOORE, D.W. 1963 The boundary layer on a spherical gas bubble. *J. Fluid Mech.* **16** (2), 161–176.
- MORDANT, N., METZ, P. & MICHEL, O. 2001 Measurement of Lagrangian velocity in fully developed turbulence. *Phys. Rev. Lett.* **21**, 214501.
- OLIVIERI, S., PICANO, F., SARDINA, G., IUDICONE, D. & BRANDT, L. 2014 The effect of the basset history force on particle clustering in homogeneous and isotropic turbulence. *Phys. Fluids* **26** (4), 041704.
- PRAKASH, V.N., TAGAWA, Y., CALZAVARINI, E., MERCADO, J.M., TOSCHI, F., LOHSE, D. & SUN, C. 2012 How gravity and size affect the acceleration statistics of bubbles in turbulence. *New J. Phys.* **14** (10), 105017.
- QURESHI, N.M., ARRIETA, U., BAUDET, C., CARTELLIER, A., GAGNE, Y. & BOURGOIN, M. 2008 Acceleration statistics of inertial particles in turbulent flow. *Eur. Phys. J. B* **66** (4), 531–536.
- RIVERO, M., MAGNAUDET, J. & FABRE, J. 1991 Quelques résultats nouveaux concernant les forces exercées sur une inclusion sphérique par un écoulement accéléré. *C. R. Acad. Sci. Paris* **312** (Série II), 1499–1506.
- RYBCZYNSKI, W. 1911 On the translatory of a fluid sphere in a viscous medium. *Bull. Acad. Sci. Cracovie A*, 40–46.
- SAWFORD, B.L. & YEUNG, P.K. 2011 Kolmogorov similarity scaling for one-particle Lagrangian statistics. *Phys. Fluids* **23** (9), 091704.
- SAWFORD, B.L., YEUNG, P.K., BORGAS, M.S., VEDULA, P., LA PORTA, A., CRAWFORD, A.M. & BODENSCHATZ, E. 2003 Conditional and unconditional acceleration statistics in turbulence. *Phys. Fluids* **15** (11), 3478–3489.
- SCHILLER, L. & NAUMANN, A. 1933 Über die grundlegenden berechnungen bei der schwerkraftaufbereitung. *Z. Verein. Deutsch. Ing.* **77**, 318–320.
- STOKES, G. 1851 On the effect of the inertial friction of fluids on the motions of pendulums. *Trans. Camb. Phil. Soc.* **9**, 8.
- TAYLOR, T.D. & ACRIVOS, A. 1964 On the deformation and drag of a falling viscous drop at low Reynolds number. *J. Fluid Mech.* **18** (3), 466–476.
- TCHEN, C.M. 1947 Mean value and correlation problems connected with the motion of small particles suspended in a turbulent fluid. PhD thesis, Delft University, Netherlands.
- TOSCHI, F. & BODENSCHATZ, E. 2009 Lagrangian properties of particles in turbulence. *Annu. Rev. Fluid Mech.* **41** (1), 375–404.
- VOLK, R., CALZAVARINI, E., LÉVÊQUE, E. & PINTON, J.-F. 2011 Dynamics of inertial particles in a turbulent von Kármán flow. *J. Fluid Mech.* **668**, 223–235.
- VOLK, R., CALZAVARINI, E., VERHILLE, G., LOHSE, D., MORDANT, N., PINTON, J.-F. & TOSCHI, F. 2008 Acceleration of heavy and light particles in turbulence: comparison between experiments and direct numerical simulations. *Physica D* **237** (14–17), 2084–2089.
- VOTH, G.A., LA PORTA, A., GRAWFORD, A.M., ALEXANDER, J. & BODENSCHATZ, E. 2002 Measurements of particle accelerations in fully developed turbulence. *J. Fluid Mech.* **469**, 121.
- WANG, L.-P. & MAXEY, M.R. 1993 Settling velocity and concentration distribution of heavy particles in homogeneous isotropic turbulence. *J. Fluid Mech.* **256**, 27–68.
- YEUNG, P.K., POPE, S.B., LAMORGESE, A.G. & DONZIS, D.A. 2006 Acceleration and dissipation statistics of numerically simulated isotropic turbulence. *Phys. Fluids* **18**, 065103.
- ZHANG, Z. 2019 Dynamique des micro-bulles dans un écoulements turbulents. PhD thesis, Institut National Polytechnique de Toulouse.
- ZHANG, Z., LEGENDRE, D. & ZAMANSKY, R. 2019 Model for the dynamics of micro-bubbles in high Reynolds number flows. *J. Fluid Mech.* **879**, 554–578.